Mathematical investigation of ellipsoidal particles separation in the hydrocyclones

O V Matvienko [1,2]
[1]Tomsk State University of Architecture and Building, Department of theoretical mechanics, Tomsk, 634003, Russia

[2] National Research Tomsk State University, Department of Physical and Computational Mechanics, Tomsk, 634050, Russia

E-mail: matvolegv@mail.rul

Abstract. This paper presents the results of the numerical studies of the non-spherical particles separation in the hydrocyclones. The calculations are done for freely rotating particles, and particles with orientations fixed by means of an external torque exerted by a strong orienting field. The results demonstrate that separation characteristics of the hydrocyclone are strongly depends on the flow shear rate, particle size, and particle shape. The model is validated by the good agreement between the measured and predicted results.

1. Introduction

Hydrocyclones are used extensively for particle separation and classification in mineral, environmental and chemical engineering. The popularity of the hydrocyclone can be described to its simplicity, ease of operation, small physical size in proportion to the high volumetric throughputs that it can handle and the relatively low capital, operating and maintenance costs associated with its use.

Figure 1. General view of the hydrocyclone.

A typical hydrocyclone consists of a cylindrical section with a central tube connected to a conical section with a discharge tube (Figure 1). An inlet tube is attached to the top section of cylinder at the point of entry. Two exits, at the top (or overflow) and bottom (or underflow) of the cyclone yield the

separation products together with a carried liquid. The fluid being injected tangentially into the hydrocyclone causes swirling within device, thus generating centrifugal force. Under the influence of different centrifugal forces, the heavy phase is pushed towards the wall and then leaves the hydrocyclone through the underflow; the light phase towards the cyclone axis, where it joins the up wards flow in a central vortex, leaves the cyclone through the overflow [1].

In recent years, alongside the traditional application of hydrocyclones in mineral processing, new applications, particularly in the field of environmental engineering, have opened up for these separators. Examples in this context include their application for gypsum separation in wet flue gas desulphurization processes, in washing plants for contaminated soils and in separation plants for tunnel driving projects. To ensure that the potential of hydrocyclone engineering is fully utilized, the optimum hydrocyclone geometry specific to the respective application, the correct combination of materials and appropriate operating parameters are essential. Extensive experiments in pilot scale are therefore required in the planning phase. The effort involved in this process can be reduced substantially with the help of modern computational engineering.

The flow behavior in hydrocyclone is quite complex. This complexity of flow processes has led designers to rely on empirical equations for predicting the equipment performance. These empirical relationships are derived from an analysis of experimental data and include the effect of operational and geometric variables. Different sets of experimental data lead to different equations for the same basic parameters. Empirical models correlate with classification parameter, such as the cut size with device dimensions and slurry properties [2].

The first successful work in predicting the fluid flow in hydrocyclones is the one of Pericleous and Rhodes [3], who used the PHOENICS computer code for the solution of the partial differential equations. Using the simple Prandtl mixing length model and the axisymmetry assumptions, the authors reported the velocity predictions in a 200-mm hydrocyclone. Later, Hsieh and Rajamani (1991) numerically solved the turbulent momentum equations to obtain the velocities and compared them with the Laser Doppler Velocimetry measurements in a 75-mm hydrocyclone. Numerical calculations of the separation of suspensions with different particle size distribution in the hydrocyclone show that feed solid concentration affects the separation parameters of the hydrocyclone [4].

The influence of the presence of an air column in a hydrocyclone and the regime of flow of particles through its discharge orifices on the separation characteristics of the hydrocyclone was investigated in paper [5, 6]. It was established that the flow of heavy particles through the lower discharge orifice of the hydrocyclone in the case where its upper discharge orifice is isolated from the atmosphere is larger than that in the case of free flow of particles to the atmosphere though both two orifices of the hydrocyclone. In the case where the lower discharge orifice of the hydrocyclone is isolated from the atmosphere, the involvement of light particles from the lower receiving bin into the reverse fluid flow in the axial zone of the hydrocyclone increases the resulting yield of particles through the upper discharge orifice of the hydrocyclone.

The majority of experimental and theoretical investigations use spherical particles. However, in a number practical situations particle shape deviates from spherical, either being irregular or having a well-defined geometry, such as granulates or fibers. The goal of this paper is to analyze the hydrodynamics, non-spherical particles motion and its separation in the hydrocyclone.

2. Mathematical model

The equations required for the description of the flow patterns in vortex devices express the time averaged fluid flow balance of mass and momentum. These equations are given here in cylindrical coordinates, which are best suited to the geometry of the conventional hydrocyclone. The parameters of the flow depend on the solid concentration and the density and viscosity of the slurry. It is assumed that particles concentrated suspension influence fluid velocities via density and viscosity. The

turbulent Reynolds equations used for description of the flow fields, written in time-averaged variables have the following form:

$$\frac{\partial \rho u}{\partial x}+\frac{1}{r}\frac{\partial \rho v r}{\partial x}=0\,, \tag{1}$$

$$\frac{\partial \rho u^2}{\partial x}+\frac{1}{r}\frac{\partial \rho u v r}{\partial r}=-\frac{\partial p}{\partial x}+\frac{\partial}{\partial x}\left[\mu_{eff}\left(2\frac{\partial u}{\partial x}-\frac{2}{3}\left(\frac{\partial u}{\partial x}+\frac{1}{r}\frac{\partial v r}{\partial r}\right)\right)\right]+\frac{1}{r}\frac{\partial}{\partial r}\left[\mu_{eff} r\left(\frac{\partial u}{\partial r}+\frac{\partial v}{\partial x}\right)\right], \tag{2}$$

$$\frac{\partial \rho u v}{\partial x}+\frac{1}{r}\frac{\partial \rho v^2 r}{\partial r}=-\frac{\partial p}{\partial r}+\frac{\partial}{\partial x}\left[\mu_{\text{eff}}\left(\frac{\partial v}{\partial x}+\frac{\partial u}{\partial r}\right)\right]+ +\frac{1}{r}\frac{\partial}{\partial r}\left[\mu_{\text{eff}} r\left(2\frac{\partial v}{\partial r}-\frac{2}{3}\left(\frac{\partial u}{\partial x}+\frac{1}{r}\frac{\partial v r}{\partial r}\right)\right)\right]-2\frac{\mu_{\text{eff}} v}{r^2}+\frac{\rho w^2}{r}\,, \tag{3}$$

$$\frac{\partial \rho u w}{\partial x}+\frac{1}{r}\frac{\partial \rho v w r}{\partial x}=\frac{\partial}{\partial x}\left[\mu_{\text{eff}}\frac{\partial w}{\partial x}\right]+\frac{1}{r^2}\frac{\partial}{\partial r}\left[\mu_{r\varphi} r^3\frac{\partial}{\partial r}\left(\frac{w}{r}\right)\right]-\frac{\rho v w}{r}\,. \tag{4}$$

Here *u, v, w* are velocity components, p is pressure, x, r are the axial and radial co-ordinates, x, r are the axial and radial coordinate.

The turbulence characteristics were calculated on the basis of two-equation k - ε model (k being the turbulent energy, ε is the turbulence dissipation rate) with a Richardson numbers correction to the dissipation equation with the turbulent viscosity for the swirl equation reduced by a factor of $\sigma_{r\varphi}$:

$$\frac{\partial \rho u k}{\partial x}+\frac{1}{r}\frac{\partial \rho v k r}{\partial x}=\frac{\partial}{\partial x}\left[\frac{\mu_{\text{eff}}}{\sigma_k}\frac{\partial k}{\partial x}\right]+\frac{1}{r}\frac{\partial}{\partial r}\left[\frac{\mu_{\text{eff}}}{\sigma_k} r\frac{\partial k}{\partial r}\right]+G-\rho\varepsilon-D\,, \tag{5}$$

$$\frac{\partial \rho u \varepsilon}{\partial x}+\frac{1}{r}\frac{\partial \rho v \varepsilon r}{\partial x}=\frac{\partial}{\partial x}\left[\frac{\mu_{\text{eff}}}{\sigma_\varepsilon}\frac{\partial \varepsilon}{\partial x}\right]+\frac{1}{r}\frac{\partial}{\partial r}\left[\frac{\mu_{\text{eff}}}{\sigma_\varepsilon}\frac{\partial \varepsilon}{\partial r}\right]+\left(C_1-C_2\rho\varepsilon\right)\frac{\varepsilon}{k}+E\,, \tag{6}$$

$$G=\mu_t\left\{2\left[\left(\frac{\partial u}{\partial r}\right)^2+\left(\frac{\partial v}{\partial r}\right)^2+\left(\frac{v}{r}\right)^2\right]+\left(\frac{\partial u}{\partial r}+\frac{\partial v}{\partial x}\right)^2+\left(\frac{\partial w}{\partial x}\right)^2+\left(r\frac{\partial w/r}{\partial r}\right)^2\right\}, \tag{7}$$

$$D=2\mu\left[\left(\frac{\partial\sqrt{k}}{\partial x}\right)^2+\left(\frac{\partial\sqrt{k}}{\partial x}\right)^2\right], \tag{8}$$

$$E=2\frac{\mu_0\mu_t}{\rho}\left\{\left[\left(\frac{\partial^2 u}{\partial x^2}\right)+\frac{1}{r^2}\left(\frac{\partial}{\partial r}\left(r\frac{\partial u}{\partial r}\right)\right)\right]^2+\left[\left(\frac{\partial^2 v}{\partial x^2}\right)+\frac{1}{r^2}\left(\frac{\partial}{\partial r}\left(r\frac{\partial v}{\partial r}\right)\right)\right]^2+ +\left[\left(\frac{\partial^2 w}{\partial x^2}\right)+\frac{1}{r^2}\left(\frac{\partial}{\partial r}\left(r\frac{\partial w}{\partial r}\right)\right)\right]^2\right\}, \tag{9}$$

$$Ri_g=\frac{2\mu w}{G}\frac{\partial}{\partial r}\left(\frac{w}{r}\right),\qquad Ri_t=\frac{k^2}{\varepsilon^2}\frac{w}{r^2}\frac{\partial(wr)}{\partial r}\,. \tag{10}$$

Here the following designation is used: μ_{eff} is effective viscosity equal to the sum of the slurry μ and turbulent $\mu_t=C_\mu f_\mu \rho k^2\varepsilon^{-1}$ viscosities. The values of constants are: $C_\mu=0.09$, $C_1=1.44\left(1+C_3 Ri_g\right)$, $C_2=1.92\left(1-C_4\mathrm{Ri}_t\right)$, $C_3=0.9$, $C_4=0.001$, $C_\mu=0.09$, $\sigma_k=1$, $\sigma_\varepsilon=1.3$, $\sigma_{r\varphi}=2.5$, $f_\mu=exp\left(-3.4/\left(1+0.02Re_t\right)^2\right)$, $Re_t=\rho k^2/\mu\varepsilon$.

From a mathematical point of view, the set of equations presented above is of an elliptical type and requires boundary conditions to be specified at all surfaces constraining the flow. Wall functions were

employed to calculate the velocities and turbulence parameters in the vicinity of the wall. The boundary conditions at the inlet are specified once for all variables. To be able to treat the problem in two-dimensions, the fluid was assumed to be inlet into the cyclone chamber through a circumferential slot, the width of which was adjusted so that the flow rate and the inlet velocities matched the experimental conditions. The ratio of tangential to radial velocity component at the inlet was of the order 10. The inlet turbulent kinetic energy is assumed to be proportional to kinetic energy of the mean flow in the inlet tube. Zero gradient type conditions are assumed on the axis of symmetry of hydrocyclone for axial velocity, turbulent energy, dissipation and particles concentration, the tangential and radial components of velocity are zero by virtue of symmetry. On the walls of hydrocyclone velocity components equal zero. To calculate the turbulent parameters we assume the local equilibrium in the near-wall region. At the exit plane, for both overflow and underflow the gradients of the tangential velocity, turbulence parameters and particles concentrations where assumed to vanish in the axial directions, thus, having no upstream influence. For radial velocity here was assumed zero conditions. The pressure at the overflow exit was fixed according to the relation:

$$p(x_{of}, r) = \int_0^r \rho w^2 (x_{of}, \xi) d\xi \tag{11}$$

and at the underflow pressure was assumed equal the environmental pressure.

The set of the equations was solved with the use of an algorithm suggested by Patankar, where the finite difference equations where obtained by integrating the differential equations over scheduled volumes which incorporated points of a staggered finite-difference grids. The continuity equation was satisfied indirectly using an iterative method named PISO.

The trajectory of the discrete phase particle is obtained by integrating the force balance on the particle, which can be written in a Lagrangian reference frame. This force balance equates the particle inertia with the forces acting on the particle, and could be written as [7]:

$$\rho_p \frac{\pi d^3}{6} \frac{du_p}{dx} = F_{Dx} + \frac{\pi d^3}{6}(\rho_p - \rho)g, \tag{12}$$

$$\rho_p \frac{\pi d^3}{6} \frac{dv_p}{dx} = F_{Dr} + \frac{\pi d^3}{6}(\rho_p - \rho)\frac{w_p^2}{r}, \tag{13}$$

$$\rho_p \frac{\pi d^3}{6} \frac{dw_p}{dx} = F_{D\varphi} - \frac{\pi d^3}{6}(\rho_p - \rho)\frac{v_p w_p}{r}, \tag{14}$$

where F_{Dx}, F_{Dr}, $F_{D\varphi}$ – are the axial, radial and tangential components of the drag force.

We consider the ellipsoidal particle described by

$$\frac{\xi^2}{a_1^2} + \frac{\eta^2}{a_2^2} + \frac{\zeta^2}{a_3^2} = 1, \tag{15}$$

where a_1, a_2, a_3 denote the lengths of three semi-principal axes and ξ, η, ζ denotes the body-fixed coordinate system.

The drag force, acting on the particle, is related to the particle velocity by the resistance tensor $\mathbf{K}$ as: $F_{Di} = K_{ij}(v_j - v_{pj})$. For an axisymmetric particle with the symmetry axis given by the unit vector $\vec{n}$ this has the form $K_{ij} = K_1 n_i n_j + K_2(\delta_{ij} - n_i n_j)$.

Explicit results for the resistance coefficient K_1 for the motion parallel to the symmetry axis and K_2 for the motion transverse to the axis are given by the Happel and Brenner [11]. With $a_1 > a_2 = a_3$ and the aspect ratio $\lambda = a_1/a_2$, the resistance coefficients for a prolate spheroid ($\lambda > 1$) are

$$K_1 = 8\pi\pi\mu_2\tau^3\left[(2\tau^2+1)\ln(\lambda+\tau) - \lambda\tau\right]^{-1}, \qquad K_2 = 16\pi 6\pi_2\tau^3\left[(2\tau^2-1)\ln(\lambda+\tau) + \lambda\tau\right]^{-1},$$

where $\tau = \sqrt{|\lambda^2 - 1|}$.

For an oblate spheroid with $\lambda < 1$:

$K_1 = 8\pi\pi\mu_2\tau^3\left[\left(2\tau^2-1\right)\arctan\left(\lambda/\tau\right)+\lambda\tau\right]^{-1}$, $K_2 = 16\pi 6\pi_2\tau^3\left[\left(2\tau^2-1\right)\arctan\left(\lambda/\tau\right)-\lambda\tau\right]^{-1}$,

The equation of the rotational motions for spheroid is:

$$I\frac{d\vec{\omega}_p}{dt}-\left(I\cdot\vec{\omega}\right)\times\vec{\omega}=-\vec{T}. \qquad (16)$$

The relation between the external torque $\vec{T}$, the angular velocity $\vec{\omega}_p$ of the spheroid and the ambient .ow is given by:

$$T_i = \mu\left[R_1\left(\omega_{pj}-\omega_j\right)n_i n_j + R_2\left(\left(\omega_{pi}-\omega_i\right)-\left(\omega_{pi}-\omega_i\right)n_i n_j\right)\right]-\mu R_2 D\varepsilon_{ijk}E_{kl}n_j n_l \qquad (17)$$

where $D=\left(\lambda^2-1\right)/\left(\lambda^2+1\right)$, ω is the locally uniform vorticity, and E_{kl} is the locally uniform rate of strain. For a prolate spheroid:

$$R_1 = \frac{16}{3}\pi a_2^3\tau^3\left[\lambda\tau-\ln\left(\lambda+\tau\right)\right]^{-1}, \qquad R_2 = \frac{16}{3}\pi a_2^3\tau^3\left[\left(2\tau^2+1\right)\ln\left(\lambda+\tau\right)-\lambda\tau\right]^{-1}. \qquad (18)$$

For an oblate spheroid:

$$R_1 = \frac{16}{3}\pi a_2^3\tau^3\left[\arctan\left(\lambda/\tau\right)-\lambda\tau\right]^{-1}, \quad R_2 = \frac{16}{3}\pi a_2^3\tau^3\left[\left(2\tau^2-1\right)\arctan\left(\lambda/\tau\right)+\lambda\tau\right]^{-1}. \qquad (19)$$

3. Results and Discussions

The calculations were performed for a hydrocyclone with a chamber of diameter 75 mm, and diameters of underflow and overflow 12.5 mm and 25.0 mm respectively. The lengths of the cylindrical and conical parts were 100 mm and 200 mm.

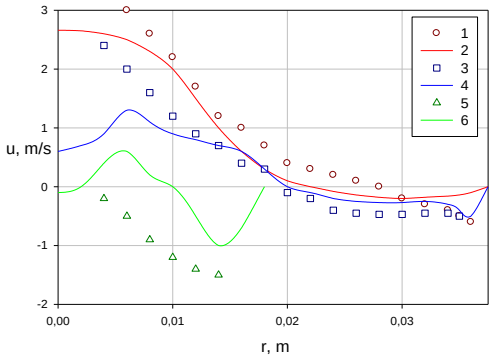

Figure 2. Radial distribution of axial velocity: 1, 3, 5 – experiment, 2. 4, 6 – calculations, 1, 2 – $x = 60$ mm, 2, 4 – $x = 120$ mm, 3, 4 – $x = 200$ mm.

On the Figure 2 one can see the calculated axial velocity distribution. It is obvious that axial velocity was positive in internal, meaning that fluid flow is upwards. In external part of the hydrocyclone axial velocity was negative, meaning that fluid flow is downwards.

The flow field in the cyclone indicates the expected forced/free combination of the Rankine vortex. The value of the tangential velocity equals zero on the wall and the centre of the flow field (air core is a forced vortex). The tangential velocity decreases as the flow spins down along the wall. Before it goes below the vortex finder, the fluid flow collides with the follow-up flow and forms a chaotic flow close to the vortex finder outside wall.

When calculating trajectories of non-spherical particles, both translational and rotational motions should be simultaneously considered, since these motions are coupled. The orientation distribution of non-spherical particles in flows is an important factor affecting the cumulative transport properties of the fluid–particle system. Lateral drift was found to occur for inertial particles with both fixed and

free orientations. For a particle with a fixed orientation the transverse motion also strongly depends on the particle orientation. The fine particles flow rate through the underflow is equal approximately to the liquid flow rate, but almost all particles with diameter more then 20 microns leave the hydrocyclone through the underflow.

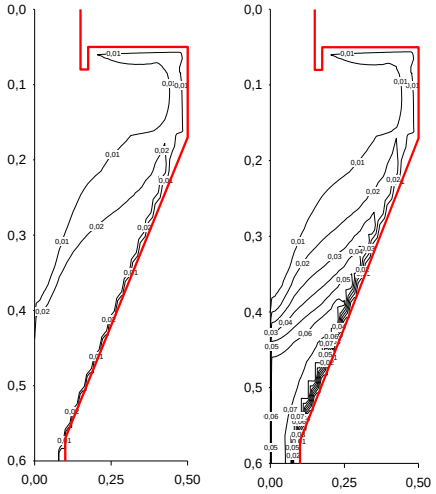

Figure 3. Particles concentration in the hydrocyclone:
$\rho_p = 1200$ kg/m^3, $d_p = 20\,\mu$m; a – $\lambda = 0.6$, b – $\lambda = 1.0$.

The decrease of the magnitude of the sphericity coefficient $\lambda = a_1/a_2$ leads to diminishing of the particles relative velocity. Therefore medium particles in the conical part of hydrocyclone cannot reach the vicinty of the wall and get with the upstream vortex in the overflow. The coarse nonspherical particles have a reduced radial displacement from the centerline. So the concentration of coarse non-spherical particles in the underflow decreasing (Figure 3).

This is mechanism for decrease the separation efficiency of the non-spherical particles. The calculations of the cut size in several hydrocyclone geometries and also particles trajectories are calculated for both inertial and inertialess particles, the orientation of which is fixed or free. The results demonstrate that separation characteristics of the hydrocyclone are strongly depends on the flow shear rate, particle size, and particle shape.

4. Conclusions

The flow in cyclones has been investigated k−ε model modified for streamline curvature effect and two Reynolds stress models. Using this model led to results that were in good agreement with experimental results. The results demonstrate that separation characteristics of the hydrocyclone are strongly dependent on the flow shear rate, particle size, and particle shape.

References

[1] Svarovsky L 1984 *Hydrocyclones* 1997-1998 (London: Technomic Publishing Co.)
[2] Fahlstrom, P H 1963 Studies of the hydrocyclone as a classifier *Proc. 6th Int. Miner. Process. Congr*. (Cannes) 211
[3] Pericleous K A, Rhodes N and Cutting G W 1984 A mathematical model for predicting the flow field in a hydrocyclone classifier *Proc. Int.Conf. Hydrocyclones* (Bath, England) 765
[4] Monredon T C, Hsieh K T and Rajamani R K 1990 Fluid flow model of the hydrocyclone: an investigation of device dimensions *Int. J. Miner. Process* **35** 143
[5] Dueck J, Matvienko O V and Neesse Th 2000 *Theor Found Chem Eng*+ **34** 478
[6] Matvienko O Dueck J 2006 *Theor Found Chem Eng*+ **40** 216
[7] Happel J and Brenner H 1986 *Low Reynolds Number* (Dordrecht: Martinus Nijhoff)